CORROSION SCIENCE AND TECHNOLOGY, Vol.23, No.3(2024), pp.203~214 pISSN 1598-6462 / eISSN 2288-6524
[Research Paper] DOI: https://doi.org/10.14773/cst.2024.23.3.203

Effects of Cladding and Antifreeze Solution on Cavitation Corrosion of AA3003 Tube of Heat Exchanger for Automobile

Young Ran Yoo[1], Seung Heon Choi[2], Hyunhak Cho[2], and Young Sik Kim[1,2†]

[1]*Materials Research Centre for Energy and Clean Technology, Andong National University, 1375 Gyeongdong-ro, Andong, 36729, Korea*

[2]*Department of Materials Science and Engineering, Andong National University, 1375 Gyeongdong-ro, Andong, 36729, Korea*

(Received May 31, 2024; Revised June 19, 2024; Accepted June 20, 2024)

A heat exchanger is a device designed to transfer heat between two or more fluids. In a vehicle's thermal management system, Al heat exchangers play a critical role in controlling and managing heat for efficient and safe operation of the engine and other components. The fluid used to prevent heat exchangers from overheating the engine is mostly tap water. Heat exchange performance can be maintained at sub-zero temperatures using a solution mixed with antifreeze. Although the fluid flowing through the heat exchanger can reduce the temperature inside the engine, it also has various problems such as cavitation corrosion. Cavitation corrosion characteristics in tap water and corrosion characteristics were evaluated in this study when antifreeze was added for test specimens where AA4045 was cladded on the inner surface of AA3003 tubes of a fin-type heat exchanger. The cavitation corrosion resistance of AA3003 was found to be superior to that of AA4045 regardless of the test solution due to higher corrosion resistance and hardness of AA3003 than those of AA4045. The cavitation corrosion rate of Al alloys increased with the addition of antifreeze.

Keywords: *Heat exchanger, Aluminum alloys, Cavitation, Corrosion, Clad materials*

1. Introduction

A heat exchanger is a device designed to transfer heat between two or more fluids. It is commonly used in heating, cooling, and air conditioning systems to regulate the temperature of fluids, thereby enhancing the system's efficiency. The development of heat exchangers focuses on increasing efficiency, reducing weight, enhancing durability, utilizing 3D printing, and promoting environmental friendliness [1-3]. Especially in the automotive industry, the use of lightweight materials such as Al can reduce the weight of heat exchangers and improve fuel efficiency [2,4].

In an internal combustion gasoline engine, the heat generated in the detonation stroke of the four stages of intake, compression, detonation and exhaust can reach 1,500 to 2,000 ℃. In a vehicle's thermal management system, Al heat exchangers play a critical role in controlling and managing heat for the efficient and safe operation of the engine and other components. Heat exchangers absorb excess heat from the engine through the coolant to maintain the engine's optimal temperature, increase performance, and extend its lifespan [5-7]. There are various types of heat exchangers such as shell and tube type, double pipe heat exchanger, plate heat exchanger, air-fin heat exchanger, spiral type and plate-fin heat exchanger [8]. Among them, air-fin heat exchangers and plate-fin heat exchangers are most commonly used in automotive thermal management systems. They consist of a tube frame through which fluid flows and several thin fins on the opposite side of the frame to increase the efficiency of the heat exchanger [3]. The fluid used to prevent the heat exchanger from overheating the engine is mostly tap water, and the heat exchange performance can be maintained at sub-zero temperatures by using a solution mixed with antifreeze [5,9,10]. The ethylene glycol contained in these antifreezes can decompose into glycol, which can accelerate the corrosion of Al, the materials of the heat exchanger, so corrosion inhibitors are added separately [10,11]. The fluid flowing through

†Corresponding author: yikim@anu.ac.kr
Young Ran Yoo: Senior Researcher, Seung Heon Choi: Ph.D. Candidate, Hyunhak Cho: Ph.D. Candidate, Young Sik Kim: Professor

the heat exchanger is responsible for reducing the temperature inside the engine, but it also accompanies various problems. Therefore, various studies are being conducted to improve its performance and reliability [12-14].

The causes of heat exchanger failure can be divided into internal and external factors. External factors include the exposure of the heat exchanger to the moisture environment due to external temperature differences during operation, and failure cases caused by the formation of corrosive environments from road pollution or winter de-icing agents. To protect against corrosive environments, sacrificial anode materials are used in cladding, and studies have been conducted to delay the corrosion of heat exchangers by evaluating the electrochemical galvanic corrosion behavior [15]. The clad applied to fins and tubes to delay the development of pinholes in heat exchanger tubes exhibits sacrificial galvanic effects, the main factors influencing galvanic corrosion dissolution were determined to be galvanic corrosion potential difference and galvanic corrosion current density [15].

Internal factors causing heat exchanger failure include the ingress of corrosive substances such as sulfur and chlorine, which are detrimental to Al, and mechanical erosion caused by cavitation due to fluid flow and velocity. The presence of Cl ions in Al is known to significantly affect the corrosion of Al alloys [10,16]. It is recommended to use distilled water because even ordinary tap water contains chloride, which is corrosive, and calcium and magnesium, which can precipitate, which are potential corrosion sources [10]. Additionally, cavitation erosion can also occur due to the fluid flowing inside, and the higher the fluid velocity, the more severe the damage [17,18]. The degree of cavitation damage depends on the viscosity of the fluid, with higher viscosity leading to greater cavitation damage [19,20]. Keeping the surfaces clean and free of impurities inside the heat exchanger can somewhat reduce the risk of cavitation corrosion [21].

On the other hand, the Al alloy used inside the heat exchanger tube is a multilayer Al alloy sheet (herein referred to as Al brazing sheets) are comprised of at least two Al alloy layers roll-bonded together. The core alloy is often a 3xxx series Mn-rich Al alloy, which remains solid throughout processing of the sheet and provides the necessary strength for the assembly. Additionally, AA3xxx alloys are Al-Mn alloys that can maintain corrosion resistance due to manganese's solid solution hardening of manganese, and have excellent machinability [22]. The clad layer is an Al-Si 4xxx alloy, which melts to provide filler metal for brazed joints in the assembly when the sheet is placed in the furnace, due to the melting point depressant effect of Si on Al. The use of Al brazing sheet allows multiple joints to be created simultaneously in complex assemblies (e.g., those with internal joints) without the need to place filler metal at joint locations as an additional step during assembly [23,24]. AA4xxx alloys are Al-Si alloys, which are known to have excellent wear resistance due to the addition of Si [22]. As manufacturers strive to reduce vehicle weight without sacrificing performance, Al brazing sheets of reduced gauge thickness are increasingly used [2].

In this study, we evaluated the cavitation corrosion characteristics in tap water and analyzed the corrosion characteristics when antifreeze was added, for test specimens where AA4045 material was cladded on the inner surface of AA3003 material tubes of a fin-type heat exchanger.

2. Experimental Methods

2.1 Specimen

The specimen used for the cavitation corrosion test was an Al alloy (AA3003 /AA4045) made of AA3003 [1.26 mm thick], a commercially available Al-Mn alloy, clad with AA4045, an Al-Si alloy (the cladding was performed on a commercial heat exchanger manufactured by Company H in Korea). Table 1 shows the composition and melting point of the Al alloys used in this study.

Table 1. Chemical composition of aluminum alloys and their melting points

	Si	Fe	Cu	Mn	Zn	Ti	Al	Melting point (°C)
AA3003	0.76	0.50	0.83	1.32	0.03	0.09	Bal.	654
AA4045	9.68	0.14	-	-	0.01	-	Bal.	590

Fig. 1 shows cross-sections of the heat exchanger tubes used in this study. Fig. 1a shows the AA3003 tube cross-section and fluid, while Fig. 1b shows the cross-section and fluid with AA4045 cladding on the inner surface of the AA3003 tube. The cladding thickness was 80 μm.

2.2 Cavitation corrosion test

The cavitation corrosion test was performed using a magnetostrictive driven apparatus (R&B-RB111-CE, R&B, South Korea) built according to ASTM G32 standard [25]. The ultrasonic transducer of the cavitation corrosion test device is 20 KHz ±5% and the power output is adjustable within the range of 250 to 1,000 W. The horn tip used in the test was made of super stainless steel (Fe-25.8Cr-2.3Mo-0.2W-0.5Si-10.7Ni-0.65 Mn-0.03C-0.42N, PRE 40.44) with a diameter of 16 mm. The distance between the horn tip and the specimen was fixed at 500 μm. Freshly ground horn tips were used in all cavitation corrosion tests [26].

After the specimen was fixed in the reaction cell, it was filled with the test solution and the test temperature was respectively controlled at 20 ºC, 40 ºC, and 60 ºC (the temperature of the solution may rise due to heat generation during the cavitation corrosion test, so the chiller was automatically controlled). Corrosion rate was determined as the weight loss divided by the exposure surface area. Two types of test solutions were used: 100% tap water and a 5:5 mixture of tap water and antifreeze (50% tap water + 50% antifreeze), and the composition of the tap water and antifreeze is shown in Table 2 and 3.

The cavitation corrosion test was performed for 2 h with the ultrasonic amplitude adjusted to 5 μm, 15 μm and 25 μm. After the test, the specimens were rinsed with running water and ultrasonically cleaned in ethyl alcohol for 10 minutes. After drying the specimens, the corrosion rate was calculated using the weight loss from the initial weight using an electronic balance.

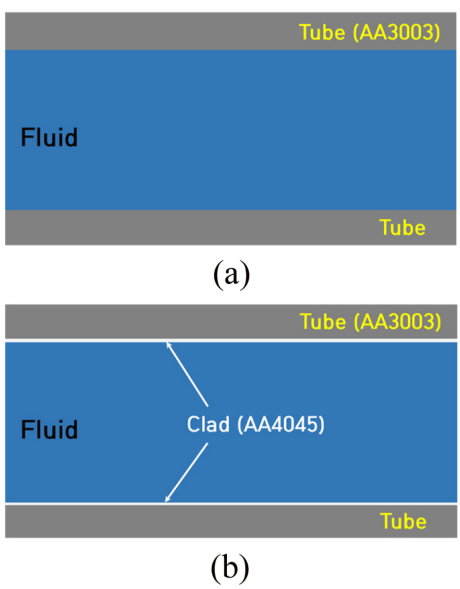

Fig. 1. Schematic diagram of cross-section of heat exchanger tube; (a) AA3003 tube without cladding (b) AA3003 tube cladded with AA4045

2.3 Appearance Observation

The appearance after the cavitation corrosion test was observed using a digital camera (Galaxy S9+, Samsung, South Korea). Additionally, the erosion damage depth on the specimen surface after the cavitation corrosion test was measured using a 3D video microscope (Hirox, KH-7700, Japan).

The appearance of the specimens before and after the cavitation corrosion test was observed using FE-SEM (Tescan, LYRA 3 XMH, Czech Republic) for the base material and cavitation zone, and the composition was analyzed using EDS (Tescan, VEGA II LMU, Czech Republic).

Table 3. Composition of antifreeze solution

Chemical substance	Chemical formula	Content, wt%
Mono Ethylene Glycol	MEG	94-95
Triethanolamine	TEA	1
Sodium hydroxide	NaOH	1
Sodium Gluconate	$NaC_6H_{11}O_7$	1
Phosphoric Acid	H_3PO_4	1

Table 2. Quality analysis of tap water in Andong city, South Korea

Tap Water	Quality Analysis			
	Residual Chlorine	Turbidity	pH	Bacteria
Average	0.25 ppm	0.09 NTU	7.1	0 CFU/mL

NTU: Nephelometric turbidity unit, CFU: Colony forming unit.

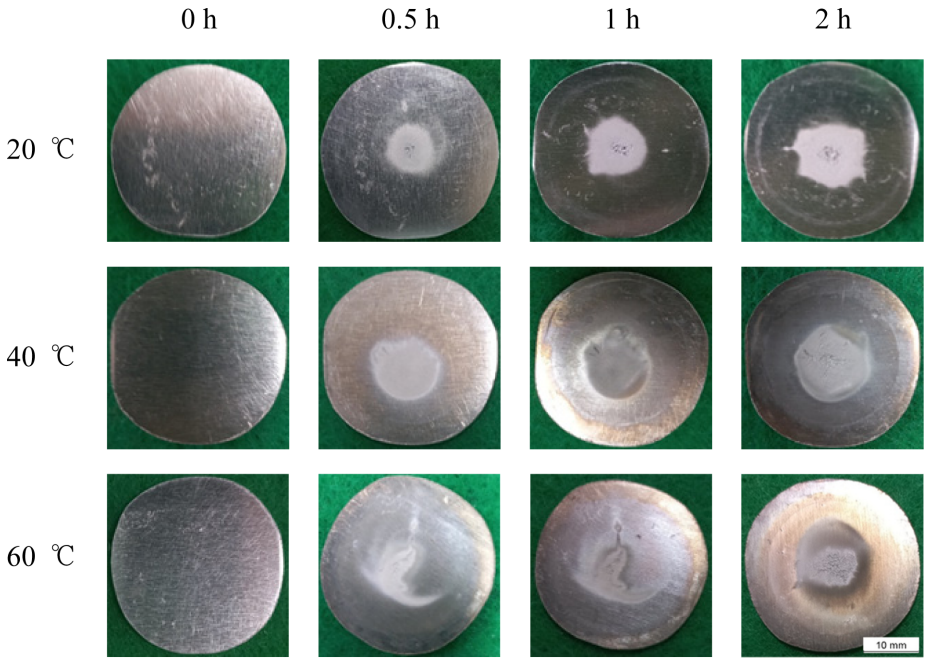

Fig. 2. Effect of solution temperature on the surface morphology of AA3003 after cavitation corrosion tests with time in tap water without antifreeze (Ultrasonic amplitude; 25 μm)

2.4 Mechanical tests

2.4.1 Continuous Indentation Hardness Test

The cross-sectional hardness of the specimens was measured using a NanoFlip Nanoindenter (KLA-NanoFlip, KLA, USA). The cross-section of the specimens was polished to a mirror finish, and a Berkovich indenter tip (with a total included angle of 142.3 degrees and a half-angle of 65.27 degrees) was used. The maximum indentation depth was 1 μm, and multiple indentations were conducted 25 times, with each indentation spaced 20 μm apart.

2.4.2 Vickers Hardness Test

The surface hardness of the specimens was measured using a Vickers Hardness Tester (HV-100, Mitutoyo, Japan). A diamond pyramid indenter was used, and the hardness value was calculated by dividing the load of 1 kgf by the area of the contact surface between the indenter and the specimen.

3. Results

The cavitation corrosion test conditions used two solutions: tap water and a 1:1 mixture of tap water and antifreeze at temperatures of 20 ºC, 40 ºC and 60 ºC. Cavitation amplitudes of 5 μm, 15 μm, and 25 μm were applied at 20 kHz, and tests were performed for 30, 60, and 120 minutes.

Fig. 2 shows the effect of solution temperature on the surface morphology of AA3003 after cavitation corrosion tests with time in tap water without antifreeze (Ultrasonic amplitude; 25 μm). Regardless of the temperature of the test environment, the cavitation affected area widened and the corrosion accelerated as the test time progressed. The cavitation corrosion test results of AA4045 evaluated under the same conditions also showed similar behavior as shown in Fig. 2.

Fig. 3 shows the effect of ultrasonic amplitude and solution temperature on the corrosion rate of AA3003 and AA4045 clad by cavitation corrosion test in tap water without antifreeze. For AA3003, the corrosion rate increased as the cavitation amplitude increased, as shown in Fig. 3a, and the corrosion rate increased as the temperature of the test environment increased, as shown in Fig. 3b. AA4045 also showed the same trend as AA3003, that the corrosion rate increased as the cavitation amplitude increased and the temperature of the test environment increased (Fig. 3c and d). The cavitation

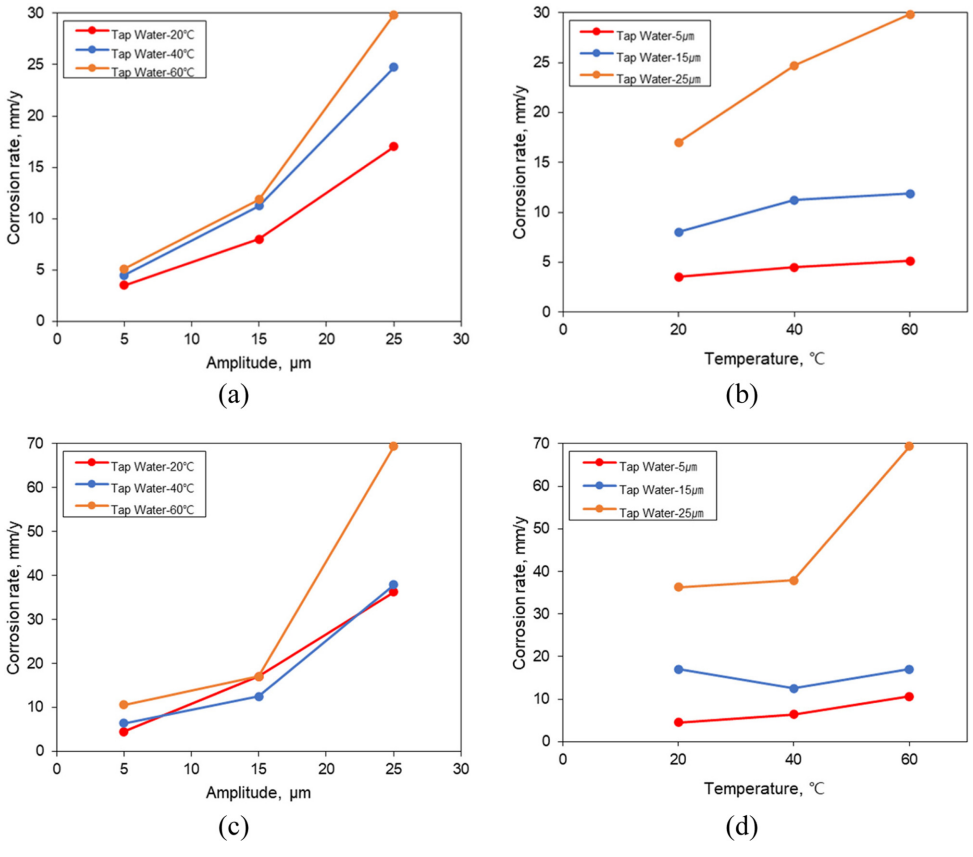

Fig. 3. Effects of (a) ultrasonic amplitude and (b) solution temperature on the corrosion rate of AA3003, and effects of (c) ultrasonic amplitude and (d) solution temperature on the corrosion rate of AA4045 clad by cavitation corrosion test in tap water without antifreeze

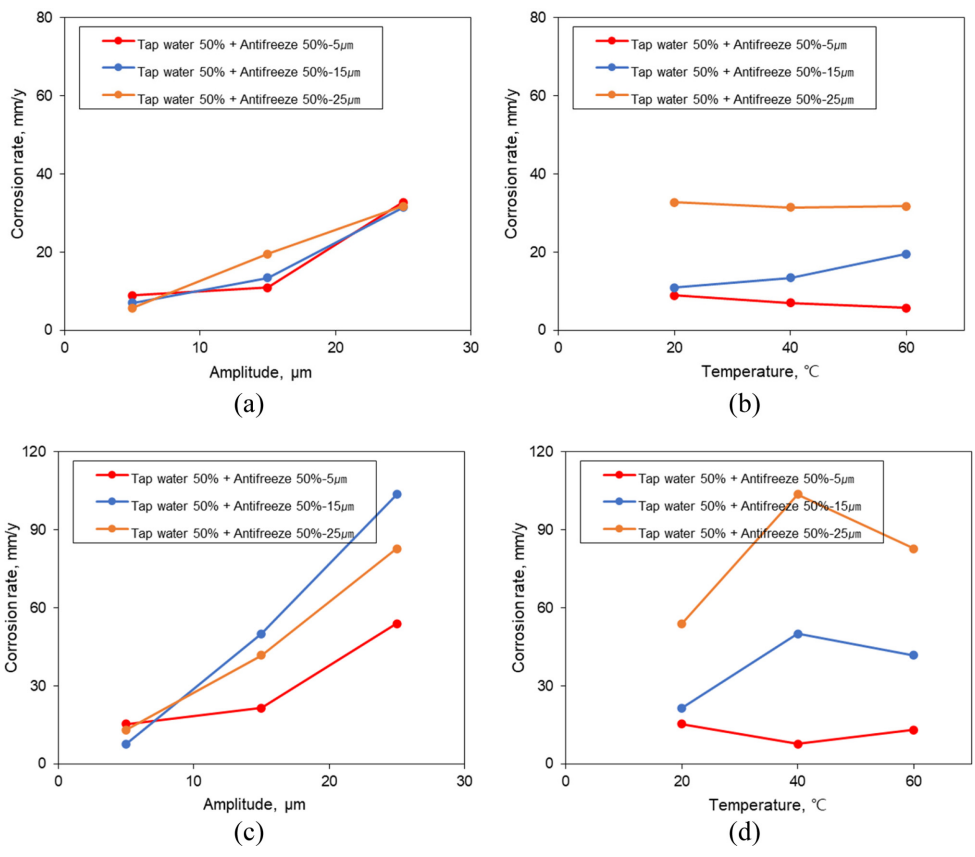

Fig. 4. Effects of (a) ultrasonic amplitude and (b) solution temperature on the corrosion rate of AA3003, and effects of (c) ultrasonic amplitude and (d) solution temperature on the corrosion rate of AA4045 clad by cavitation corrosion test in tap water with antifreeze

corrosion effects of AA3003 and AA4045 were evaluated in a mixed solution of tap water and antifreeze (50% tap water + 50% antifreeze). For both AA3003 and AA4045, the cavitation affected area widened and the corrosion

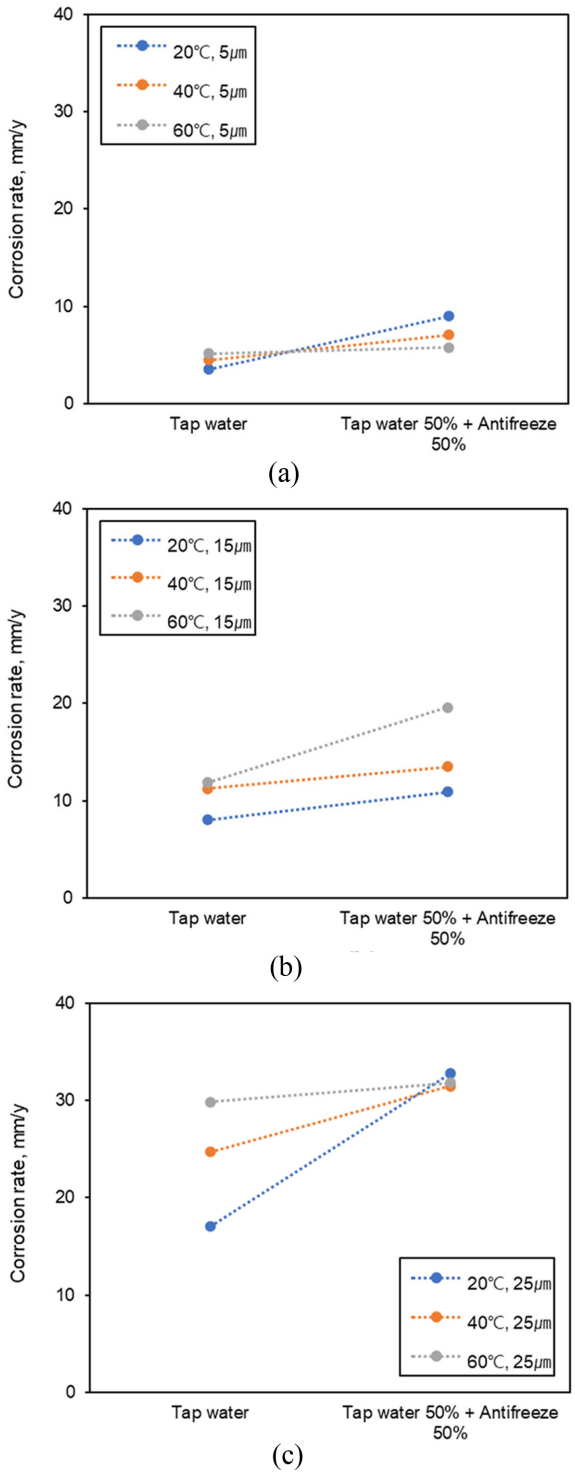

Fig. 5. Effect of antifreeze addition on the corrosion rate of AA3003 by cavitation corrosion test; (a) ultrasonic amplitude 5 μm, (b) ultrasonic amplitude 15 μm, (c) ultrasonic amplitude 25 μm

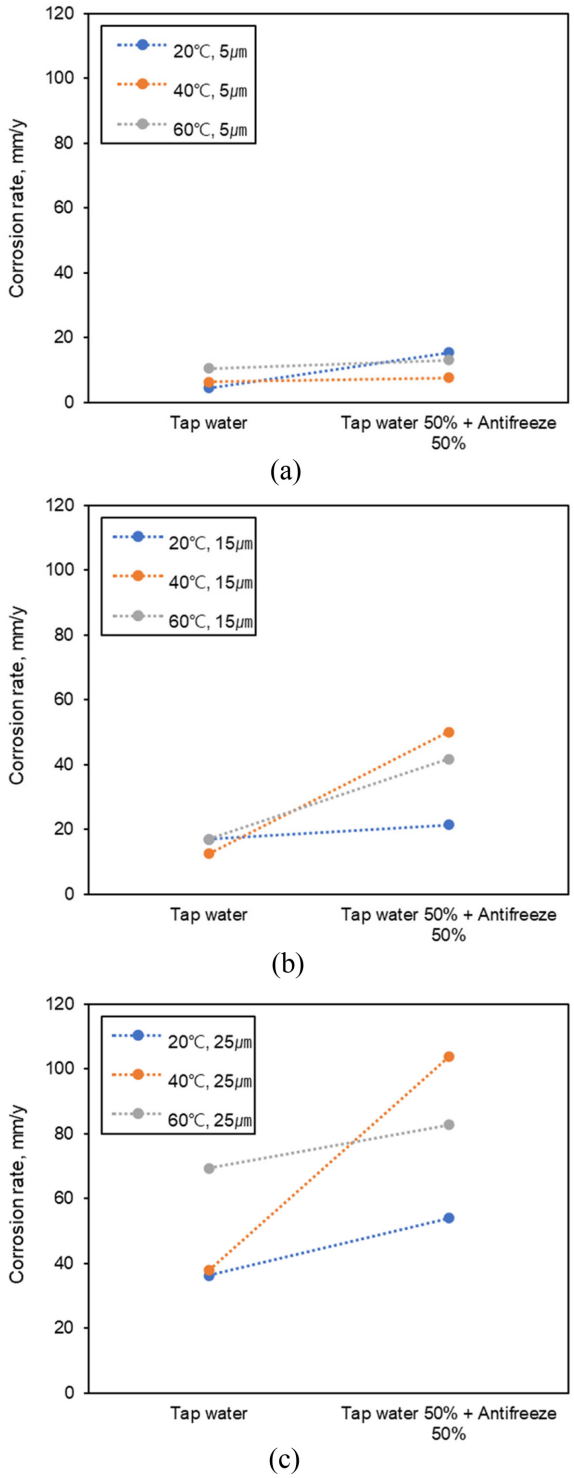

Fig. 6. Effect of antifreeze addition on the corrosion rate of AA4045 clad by cavitation corrosion test; (a) ultrasonic amplitude 5 μm, (b) ultrasonic amplitude 15 μm, (c) ultrasonic amplitude 25 μm

accelerated as the test time elapsed, showing a similar trend of appearance change as shown in Fig. 2. Fig. 4 shows the effect of amplitude (Fig. 4a, c) and test temperature (Fig. 4b, d) on the corrosion rate after cavitation corrosion test in antifreeze and tap water mixture solution of AA3003 and AA4045. For AA3003, the corrosion rate increased with increasing cavitation amplitude, but there was no obvious trend of increasing corrosion rate with increasing solution temperature. On the other hand, in the case of AA4045, the corrosion rate increased as the solution temperature increased, with a maximum corrosion rate at 40 ºC, and then the corrosion rate tended to decrease.

Fig. 5 shows the effect of antifreeze addition on the corrosion rate of AA3003 by cavitation corrosion test in

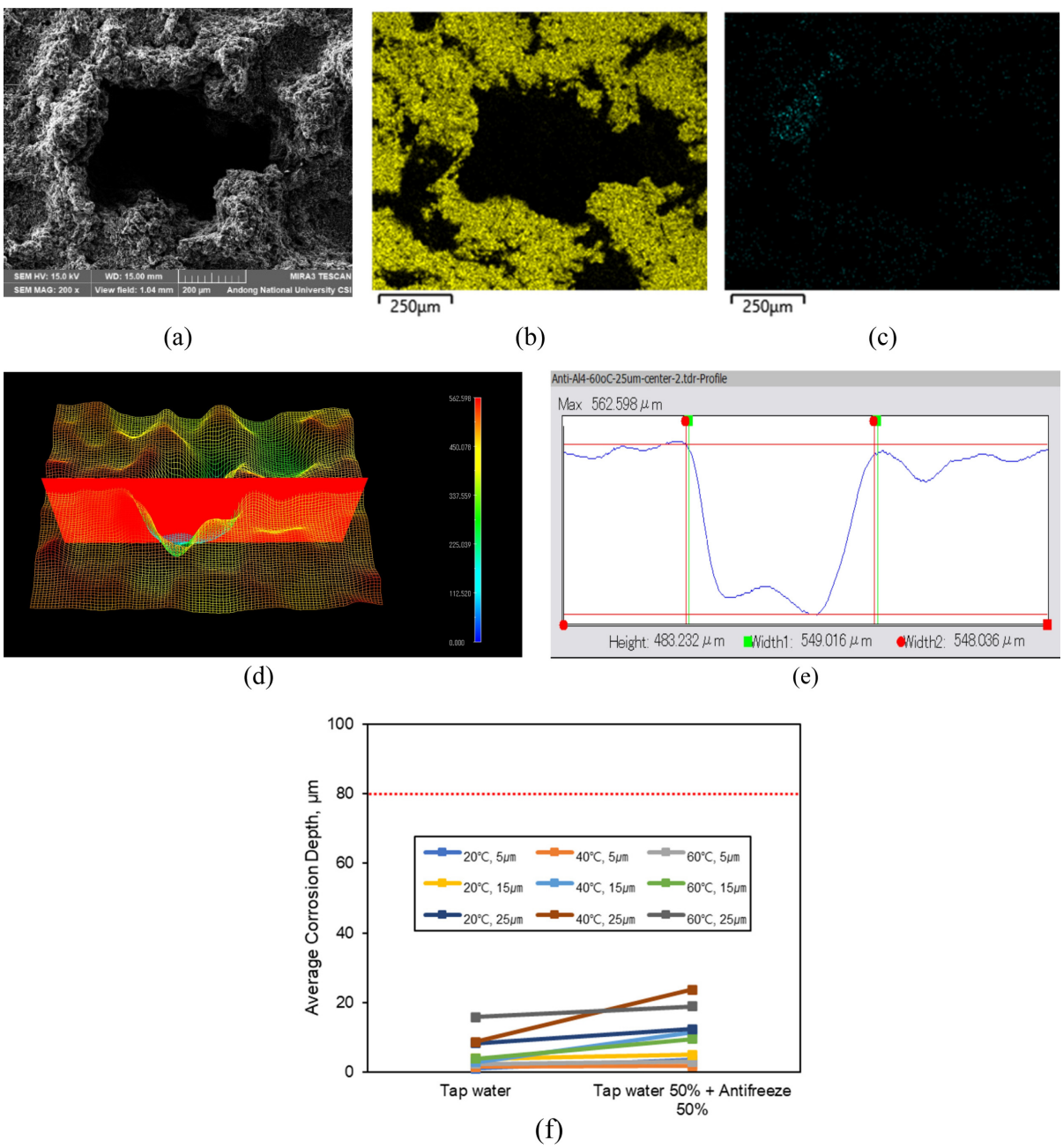

Fig. 7. (a) SEM image of AA4045 after cavitation corrosion test in 50% Tap water + 50% Antifreeze solution, (b) EDS result of Al, (c) EDS result of Si, (d) Surface contour by 3D microscope, (e) Damaged depth, (f) Average damaged depth by weight loss for 2 hours

20 ºC, 40 ºC, 60 ºC, tap water and antifreeze + tap water mixtures. For the same solution temperature and ultrasonic amplitude, the corrosion rate in antifreeze + tap water was rated higher than in tap water.

Fig. 6 shows the effect of antifreeze addition on the corrosion rate of AA4045 clad by cavitation corrosion test. The corrosion rate of AA4045 as a result of cavitation corrosion test in 20 ºC, 40 ºC, 60 ºC, tap water and antifreeze + tap water mixed solution with different ultrasonic amplitude is shown. The corrosion rate tends to increase as the ultrasonic amplitude and solution temperature increase. Also, at the same temperature and ultrasonic amplitude, the corrosion rate is higher in antifreeze + tap water than in tap water.

It is necessary to check whether the cavitation corrosion rate of the AA4045 clad obtained in the previous section has damaged the base metal AA3003 alloy under the clad layer. Fig. 7 shows the results of SEM-EDS and 3D microscopy observations of AA4045 clad material to confirm the extent of damage after cavitation test. Fig. 7a is an SEM image of the AA4045 clad surface damaged by the cavitation corrosion test. It can be seen that the cavitation corrosion has resulted in overall surface damage and localized severe fracture morphology. Fig. 7b and 7c show the Al and Si composition in the damaged area, respectively, and it can be seen that Al and Si, which are the main components of AA4045, have been lost in the severely damaged area.

Fig. 7d shows the 3D microscopy observation to measure the depth of the damage, and it can be seen that the damage is 483.2 μm deep (Fig. 7e), which exceeds the cladding thickness of 80 μm. Fig. 7f shows the average corrosion rate of AA4045 clad obtained by weight loss during the cavitation test time of 2 hours, which is less than 30 μm. In other words, the thickness reduction obtained during the cavitation corrosion test is less than the cladding thickness, but the cladding can be destroyed by localized damage as shown in Fig. 7f. However, it should be noted that the cavitation corrosion rate of AA4045 clad in this paper includes the damage of the clad material AA4045 and the base material AA3003.

4. Discussion

Effect of Alloy: Fig. 8 summarizes the effect of alloy on the corrosion rates evaluated after cavitation corrosion testing for AA3003 and AA4045 under all test conditions. It can be seen that the cavitation corrosion rate is greater for AA4045 than AA3003, regardless of the test solution. To determine the reason for this behavior, the electrochemical polarization behavior was examined in the same environment as the cavitation corrosion evaluation, and the corrosion and cavitation corrosion properties were compared.

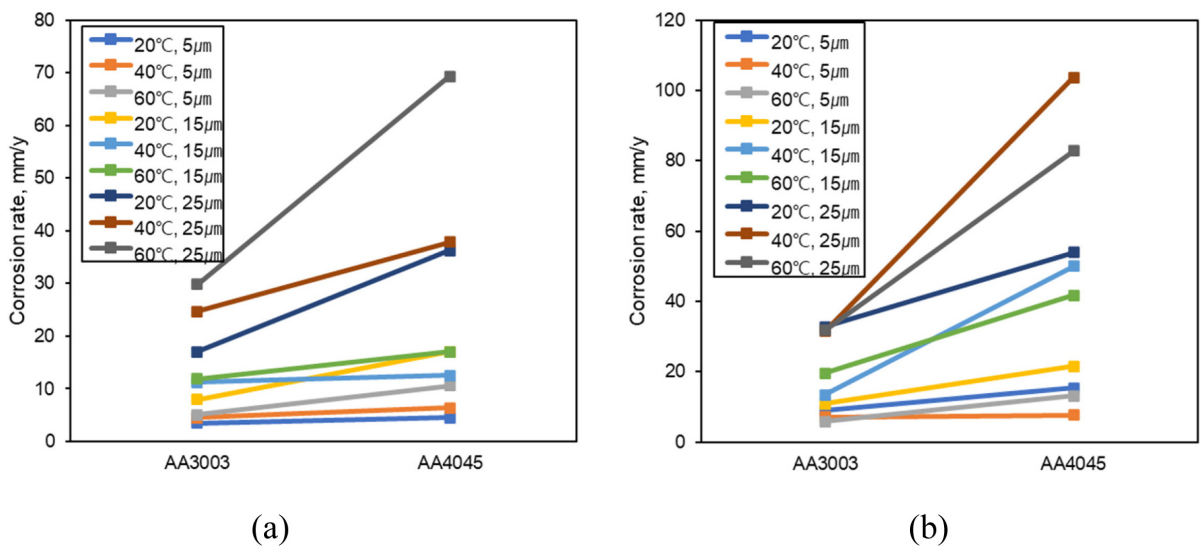

Fig. 8. Comparison of cavitation corrosion rate between AA3003 and AA4045 by cavitation corrosion test; (a) tap water without antifreeze (b) 50% tap water + 50% antifreeze solution

Fig. 9 shows the Polarization curves of AA3003 and AA4045 in tap water with and without antifreeze at 25 ºC. Both AA3003 and AA4045 exhibit superior polarization behavior in the tap water + antifreeze mixed solution compared to tap water. For both alloys, the pitting potential in the mixed solution is higher, and the passive current density is lower than in tap water. This polarization behavior is attributed to the corrosion inhibitor components contained in the antifreeze, which enhance corrosion resistance. On the other hand, considering the effect of the alloy, the polarization behavior of the base material AA3003 was evaluated to be better than that of the clad material AA4045, regardless of the solution. This is analyzed as the effect of alloying elements added to improve the corrosion resistance of Al.

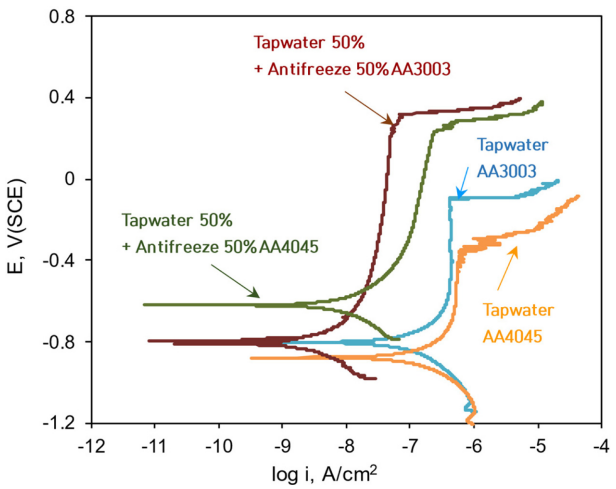

Fig. 9. Polarization curves of AA3003 and AA4045 in tap water with and without antifreeze at 25 ºC

Meanwhile, it is generally known that higher hardness is correlated with better cavitation corrosion properties in materials with similar corrosion resistance [27]. The mechanical properties for both alloys were measured and are shown in Fig. 10. Fig. 10a shows the hardness test results for the cross-section measured by the Nanofilp indentation tester, with AA3003 measured at 1.043 GPa and AA4045 at 0.880 GPa. Fig. 10b presents the surface hardness test results measured by the Vickers hardness tester, showing AA3003 with a hardness value of 48.9 HV and AA4045 with 38.5 HV, confirming that AA3003 has superior hardness compared to AA4045.

As shown in Fig. 8, the cavitation corrosion resistance of AA3003 was evaluated to be lower than that of AA4045. The reason for this result is that, as confirmed in Fig. 9, the polarization behavior of AA3003 is better than that of AA4045. Additionally, as shown in Fig. 10, the cross-sectional and surface hardness of AA3003 is higher than those of AA4045.

Influence of antifreeze: Fig. 11 shows the comparison of the cavitation corrosion rate between in tap water without antifreeze and tap water with antifreeze of AA3003 and A4045. As shown in Fig. 8, the cavitation corrosion rate of AA3003 was smaller than that of AA4045, which was analyzed to be related to its polarization properties and hardness. However, as shown in Fig. 11, regardless of the alloy, the cavitation corrosion rate in a test solution of tap water with antifreeze was

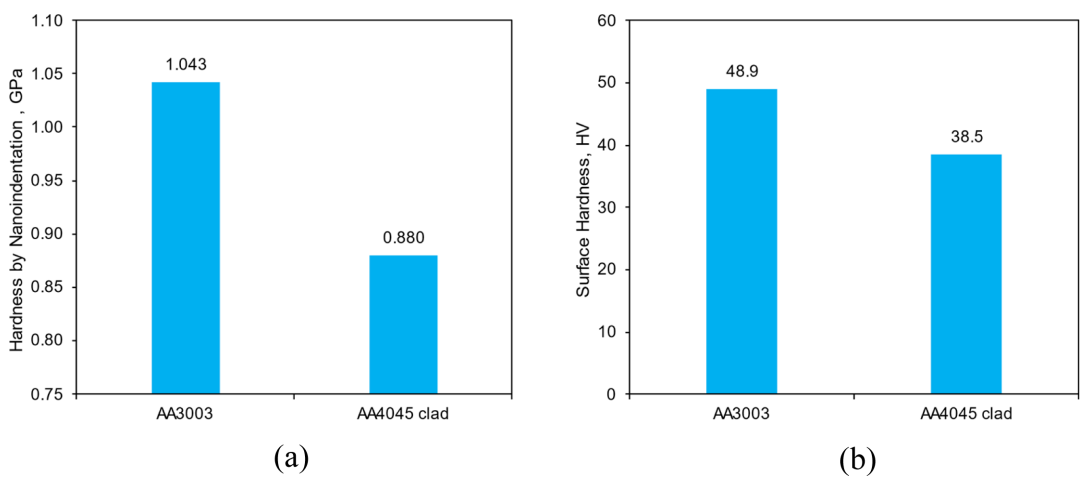

Fig. 10. Hardness on clad area of (a) cross section by Nanoflip indentation tester and (b) Vickers hardness on surface

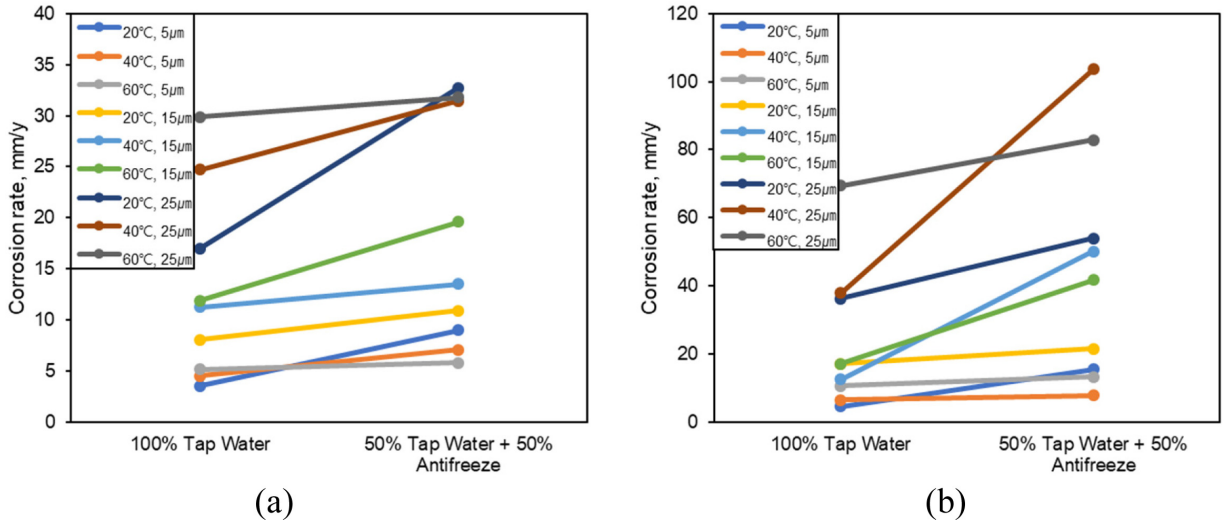

Fig. 11. Comparison of cavitation corrosion rate between in tap water without antifreeze and tap water with antifreeze; (a) AA3003, (b) AA4045

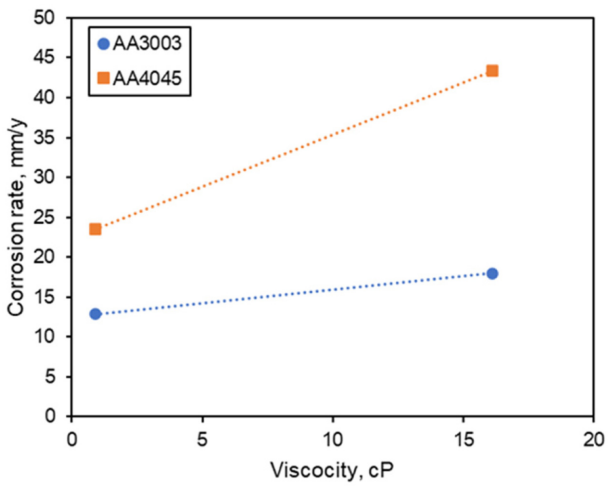

Fig. 12. Relationship between viscosity of test solutions and cavitation corrosion rate of AA3003 and AA4045

evaluated to be greater than the cavitation corrosion rate in tap water. In other words, regardless of alloy, solution temperature and ultrasonic amplitude, the cavitation corrosion rate increased with the addition of antifreeze. However, as shown in Fig. 9, it can be seen that the polarization behavior in the test solution with antifreeze was evaluated better than that in tap water. This means that it is difficult to analysis the cavitation corrosion behavior in accordance with the variation of the test solution based on the corrosion properties and hardness of the alloy only.

To analyze the cause of this behavior, the viscosity of the test solution was measured. Fig. 12 shows the cavitation corrosion rate as a function of the solution's viscosity. The solutions with significantly higher viscosity measurements were those with antifreeze added. It can be observed that as the viscosity of the solution increases, the cavitation corrosion rate also increases. The viscosity of tap water at 20 ºC is 0.9 cP, whereas the viscosity of the tap water with antifreeze is 16.1 cP. According to Wang's work [20], it is known that the cavitation area in high-viscosity solutions becomes larger and more pronounced. Therefore, the cavitation corrosion behavior of aluminum alloys with the addition of antifreeze is influenced by the viscosity of the test solution.

5. Conclusions

In this study, the cavitation corrosion properties of specimens with AA4045 material cladding on the inner surface of AA3003 tubes in a finned-tube heat exchanger were evaluated, and the effect of antifreeze addition was analyzed. The following conclusions were obtained as a result:

1. The cavitation corrosion resistance of the base material AA3003 used as the heat exchanger tube material was evaluated to be superior to that of the AA4045 cladding material regardless of the test solution, which is due to the higher corrosion resistance and hardness of AA3003 than that of the AA4045 cladding material.

2. The effect of adding antifreeze on the cavitation corrosion of Al alloys for heat exchangers was evaluated, and it was found that the cavitation corrosion rate increased with the addition of antifreeze. Despite the improvement of polarization properties due to corrosion inhibitors in antifreeze, the increase in cavitation corrosion rate is closely related to the increase in viscosity of the solution.

Acknowledgments

This research was supported by a grant from the 2023-2024 Research funds of Andong National University. And, this paper was supported by Korea Institute for Advancement of Technology (KIAT) grant funded by the Korea Government (MOTIE) (RS-2024-00409639, HRD Program for Industrial Innovation).

References

1. J. M. Kim, J. P. Lee, C. E. Lee, S. M. Kum, Characteristics of Thermal Efficiency with Changing Distances between Tubes for Heat Exchanger, *Journal of energy engineering*, **19**, 3, 177 (2010).
2. W. S Miller, L. Zhuang, J. Bottema, A. J. Wittebrood, P. De Smet, A. Haszler, A. Vieregge, Recent Development in Aluminium Alloys for the Automotive Industry, *Materials science and engineering: A*, **280**, 37 (2000). Doi: https://doi.org/10.1016/S0921-5093(99)00653-X
3. W. Faes, S. Lecompte, Z. Y. Ahmed, J. V. Bael, R. Salenbien, K. Verbeken and M. D. Paepe, Corrosion and Corrosion Prevention in Heat Exchangers, *Corrosion Reviews*, **37**, 131 (2019). Doi: https://doi.org/10.1515/corrrev-2018-0054
4. P. D. Srivyas, M. S. Charoo, Application of Hybrid Aluminum Matrix Composite in Automotive Industry, *Materials today: Proceedings*, **18**, 3189 (2019). Doi: https://doi.org/10.1016/j.matpr.2019.07.195
5. C. W. Kang, T. J. Kim, C. W. Lee, Numerical Analysis on the Characteristics of Thermal Flow in an Automobile Radiator, *Journal of the Korean Society of Manufacturing Process Engineers*, **18**, 55 (2019). Doi: https://doi.org/10.14775/ksmpe.2019.18.6.055
6. S. B. Kwak, Ph.D. Thesis, pp. 1 - 2, Hanyang University, Seoul (2011).
7. A. S. Fitrianto, C. Caing, H. A. Notonegoro, B. Soegijono, Effect of Titanium on Corrosion Behavior of Aluminum Alloy 3104 as a Candidate Material for Radiator Combustion Engines, *Flywheel*, **7**, 12 (2021). Doi: http://dx.doi.org/10.36055/fwl.v0i0.10855
8. H. M Ali, H. Ali, H. Liaquat, H. T. B. Maqsood, M. A. Nadir, Experimental Investigation of Convective Heat Transfer Augmentation for Car Radiator using ZnO-Water Nanofluids, *Energy,* **84**, 317 (2015). Doi: https://doi.org/10.1016/j.energy.2015.02.103
9. M. Asadikiya, M. Ghorbani, Effect of Inhibitors on the Corrosion of Automotive Aluminum Alloy in Ethylene Glycol-Water Mixture, *Corrosion*, **67**, 126001 (2011). Doi: https://doi.org/10.5006/1.3666860
10. O. K. Abiola, J. O. E. Otaigbe, Effect of Common Water Contaminants on the Corrosion of Aluminum Alloys in Ethylene Glycol-Water Solution, *Corrosion Science*, **50**, 242 (2008). Doi: https://doi.org/10.1016/j.corsci.2007.06.013
11. J. Zaharieva, M. Milanova, M. Mitov, L. Lutov, S. Manev, D. Todorovsky, Corrosion of Aluminum and Aluminum Alloy in Ethylene Glycol-Water Mixtures, *Journal of Alloys and Compounds*, **470**, 397 (2009). Doi: https://doi.org/10.1016/j.jallcom.2008.02.079
12. G. L. F. Mendonça, S. N. Costa, V. N. Freire, P. N. S. Casciano, A. N. Correia, and P. Lima-Neto, Understanding the Corrosion Inhibition of Carbon Steel and Copper in Sulphuric Acid Medium by Amino Acids using Electrochemical Techniques Allied to Molecular Modeling Methods, *Corrosion Science*, **115**, 41 (2017). Doi: https://doi.org/10.1016/j.corsci.2016.11.012
13. B. Jegdić, B. Bobić, and S. Linić, Corrosion Behavior of AA2024 Aluminium Alloy in Different Temperatures in NaCl Solution and with the $CeCl_3$ Corrosion Inhibitor, *Materials and Corrosion*, **71**, 352 (2020). Doi: https://doi.org/10.1002/maco.201911219
14. S. Liu J. Dong W. W. Guan J. M. Duan R. Y. Jiang Z. P. Feng and W. J. Song, The Synergistic Effect of Na_3PO_4 and Benzotriazole on the Inhibition of Copper Corrosion in Tetra-n-butylammonium Bromide Aerated Aqueous Solution, *Materials and Corrosion*, **63**, 1017 (2012). Doi: https://doi.org/10.1002/maco.201106346
15. Y. R. Yoo, D. H. Kim, G. B. Kim, S. Y. Won, S. H. Choi and Y. S. Kim, Galvanic Corrosion Between Component Parts of Aluminum Alloys for Heat Exchanger of Automobile, *Corrosion Science and Technology*, **22**, 322 (2023). Doi: https://doi.org/10.14773/cst.2023.22.5.322
16. L. Niu, Y. F. Cheng, Electrochemical Characterization of Metastable Pitting of 3003 Aluminum Alloy in Ethylene

Glycol-Water Solution, *Journal of Materials Science*, **42**, 8613 (2007). Doi: https://doi.org/10.1007/s10853-007-1841-1

17. L. Hao, F. Zheng, X. Chen, J. Li, S. Wang, Y. Fan, Erosion Corrosion Behavior of Aluminum in Flowing Deionized Water at Various Temperatures, *Materials*, **13**, 779 (2020). Doi: https://doi.org/10.3390/ma13030779
18. D. H. Kim, Y. R. Yoo, and Y. S. Kim, Effect of Water Impingement Conditions on the Degradation of Epoxy Coatings in Tap Water, *Corrosion Science and Technology*, **21**, 327 (2022). Doi: https://doi.org/10.14773/cst.2022.21.5.327
19. J. M. Nouri, l. Vasilakos, Y. Yan, Effect of Viscosity and Speed on Oil Cavitation Development in a Single Piston-Ring Lubricant Assembly, *lubricants*, **7**, 88 (2019). Doi: https://doi.org/doi:10.3390/lubricants7100088
20. L. Wang, C. Lu, The Effect of Viscosity on the Cavitation Characteristics of High Speed Sleeve Bearing, *Journal of Hydrodynamics*, **27**, 367 (2015). Doi: https://doi.org/10.1016/S1001-6058(15)60494-2
21. D. Laougli, F. Beniere, Evaluation of inhibitor efficiency on corrosion of the aluminum heat exchangers and radiators in central heating, *Journal of Materials and Environmental Science*, **3**, 34 (2012). https://www.jmaterenvironsci.com/Document/vol3/3-JMES-66-2011-Laouali.pdf
22. X. Han, H. Zhang, B. Shao, L. Li, K. Qin and J. Cui, Interfacial Characteristics and Properties of a Low-clad-ratio AA4045/AA3003 Cladding Billet Fabricated by Semi-continuous Casting, *International Journal of Minerals, Metallurgy, and Materials*, **23**, 1097 (2016). Doi: https://doi.org/10.1007/s12613-016-1327-8
23. M. J. Benoit, I. G. Ogunsanya, S. Winkler, M. J. Worswick, M. A. Wells and C. M. Hansson, Internal Corrosion of Warm Formed Aluminum Alloy Automotive Heat Exchangers. *Journal of Materials Engineering and Performance*, **30**, 2876 (2021). Doi: https://doi.org/10.1007/s11665-021-05616-4
24. American Welding Society, *Brazing Handbook, 5th ed.*, American Welding Society, Miami (2007).
25. ASTM G32-16, Standard Test Method for Cavitation Erosion Using Vibratory Apparatus, ASTM International, West Conshohocken, PA (2016). Doi: https://doi.org/10.1520/G0032-16
26. J. M. Jeon, Y. R. Yoo, M. J. Jeong, Y. C. Kim, and Y. S. Kim, Effect of Solution Temperature on the Cavitation Degradation Properties of Epoxy Coatings for Seawater Piping, *Corrosion Science and Technology*, **20**, 325 (2021). Doi: https://doi.org/10.14773/cst.2021.20.6.325
27. A. Karabenciov, A. D. Jurchela, I. Bordeasu, M. Popoviciu, N. Birau, A. Lustyan, Considerations upon the Cavitation Erosion Resistance of Stainless Steel with Variable Chromium and Nickel Content, *Earth and Environmental Science*, **12**, 012036 (2010). Doi: https://doi.org/10.1088/1755-1315/12/1/012036